Quantifying the Effects of Contact Tracing, Testing, and Containment Measures in the Presence of Infection Hotspots

Lars Lorch*, Heiner Kremer†, William Trouleau‡, Stratis Tsirtsis§, Aron Szanto¶, Bernhard Schölkopf†,*, Manuel Gomez-Rodriguez§

*ETH Zürich, llorch@student.ethz.ch
†Max Planck Institute for Intelligent Systems, {heiner.kremer,bs}@tuebingen.mpg.de
‡École Polytechnique Fédérale de Lausanne, william.trouleau@epfl.ch
§Max Planck Institute for Software Systems, {stsirtsis,manuelgr}@mpi-sws.org
¶Zerobase Foundation, aron@zerobase.io

May 19, 2021

Abstract

Multiple lines of evidence strongly suggest that infection hotspots, where a single individual infects many others, play a key role in the transmission dynamics of COVID-19. However, most of the existing epidemiological models fail to capture this aspect by neither representing the sites visited by individuals explicitly nor characterizing disease transmission as a function of individual mobility patterns. In this work, we introduce a temporal point process modeling framework that specifically represents visits to the sites where individuals get in contact and infect each other. Under our model, the number of infections caused by an infectious individual naturally emerges to be overdispersed. Using an efficient sampling algorithm, we demonstrate how to apply Bayesian optimization with longitudinal case data to estimate the transmission rate of infectious individuals at the sites they visit and in their households. Simulations using fine-grained and publicly available demographic data and site locations from Bern, Switzerland showcase the flexibility of our framework. To facilitate research and analyses of other cities and regions, we release an open-source implementation of our framework.[1]

1 Introduction

As countries around the world aim to counteract rising numbers of COVID-19 infections [1], overwhelmingly growing evidence suggests that few infected people in infection hotspots, or *superspreading events* (SSEs), may be responsible for both explosive early growth of cases and sustained transmission in later stages [2–7]. For example, in Hong Kong, the largest infection hotspots were traced back to four bars, which accounted for 32.5% of all locally acquired infections from January 23 to April 28, 2020 [2]. In South Korea, an infection hotspot linked to a church was responsible for at least 60% of all recorded cases by March 18, 2020, and over 1,000 infections were traced back to a single individual [8]. The first major outbreak in Germany occurred after an infected couple attended a carnival festivity in Heinsberg, with superspreading dynamics later verified by virus genome sequencing [9]. These lines of evidence suggest that, for COVID-19, the number of infections caused by single infectious individuals is *overdispersed*—most individuals infect few and a few infect many, exhibiting greater variance than expected under Poisson assumptions [10–12]. Using carefully annotated tracing data, this has been identified as a root cause of SSEs [2, 4–6].

Most of the existing epidemiological models, including those developed and used in the context of the COVID-19 pandemic, do not explicitly represent sites of transmission, nor do they characterize exposures as

[1]Our code is publicly available at: https://github.com/covid19-model/

a function of individual mobility patterns. Moreover, they either assume or result in a Poisson distribution of infections caused by an infectious individual, also called *secondary infections*, which fails to capture the high dispersion observed for COVID-19.[2] As a result, these models have been of little use for identifying conditions under which hotspots emerge [6, 10], helping design control measures tailored to prevent SSEs [16], or predicting where infection hotspots are most likely to occur [12].

In this work, we take a first step towards addressing the above limitations and develop a flexible temporal point process modeling framework that explicitly represents visits to sites where exposures occur. In particular, we introduce

(i) an event-based "check-in" mobility model that characterizes the frequency and duration of each individual's visits to specific sites, which can be configured using a variety of publicly available data, and

(ii) a new rate of transmission at sites that quantifies the influence of environmental drivers, individual mobility patterns, and containment measures on the risk that each infected individual poses to others at a site.

By using this novel model of transmission and an explicit representation of the visited locations, our framework can directly characterize fine-grained interventions that are, for example, targeted at particular sites or individuals (*e.g.*, hygienic measures at work places, closures of schools, or contact tracing). We derive an efficient sampling algorithm for our model, which allows us to simulate and study the spread of COVID-19 in real-world cities and regions with hundreds of thousands of inhabitants under a variety of measures and what-if scenarios. Building on this procedure, we use Bayesian optimization [17–19] in combination with longitudinal COVID-19 case data to estimate the model parameters that control the transmission of the disease.

We showcase our method using fine-grained demographic data and site locations from Bern, Switzerland, and other regions in Germany and Switzerland. Our results demonstrate that the number of individual disease transmissions—both overall and during a site visit—naturally emerges to be overdispersed, *i.e.*, exhibiting higher variance than expected under the common Poisson assumption, and that our model is able to robustly characterize the observed COVID-19 case trends. These findings hint at the potential of using our framework as a complementary policy tool for studying the efficacy of containment measures, factors of disease transmission, and the nature of infection hotspots—hand in hand with existing societal and ethical considerations. To facilitate research and analyses in this area, we release an open-source implementation of our framework [20].

2 A Spatiotemporal Epidemic Model

Given a set of individuals $\mathcal{V}$, we track the current state of each single individual $i \in \mathcal{V}$ using a collection of state variables, which determine their mobility pattern, epidemiological condition, and testing status. The state transitions are modeled using stochastic differential equations (SDEs) with jumps, which faithfully captures (i) the stochastic nature of infection events and mobility patterns, (ii) events in continuous time, i.e. *not* in aggregate over a period, and (iii) discrete state transitions—an individual either does *or* does not get infected, visit a site, or get tested positively.

Specifically, the jumps are modeled using temporal point processes [21]. A temporal point process is often represented as a counting process, say $N(t)$, which records the number of discrete events in time $\{t_1, t_2, \ldots, t_n\}$, $t_i \in \mathbb{R}_+$ before time t. The probability of an event occurring in a small time window $[t, t + dt)$ is given by $P(dN(t) = 1 \,|\, \mathcal{H}(t)) = \lambda(t)\, dt$ with $dN(t) \in \{0, 1\}$ and history of events $\mathcal{H}(t)$. The intensity function $\lambda(t)$ can be interpreted as the instantaneous rate of events per unit of time. In what follows, to ease the exposition, we describe each type of state variable separately.

2.1 Mobility

Let $\mathcal{S}$ be the set of *sites* individuals can visit. For each individual i, let the indicator $P_{i,k}(t) = 1$ if the individual is at site $k \in \mathcal{S}$ at time t and $P_{i,k}(t) = 0$ otherwise. We characterize the value of the states $P_{i,k}(t)$

[2] Overdispersion has also been observed in MERS and SARS [13–15].

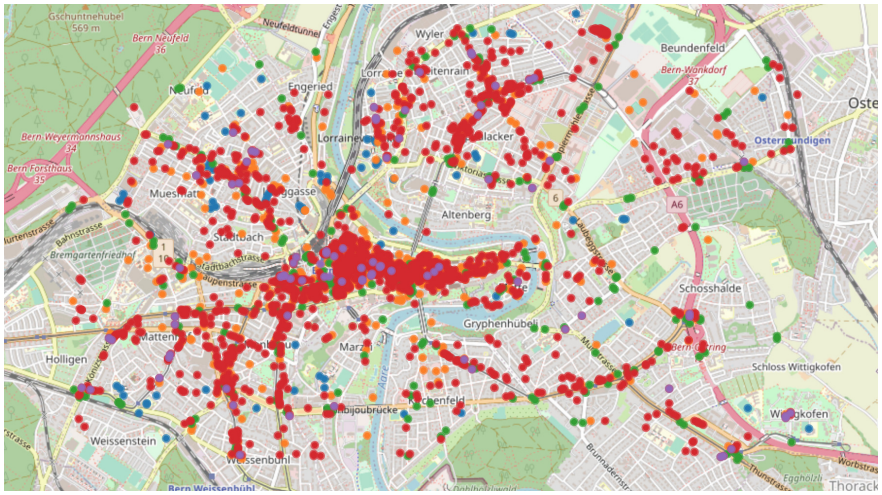

Figure 1: **Site locations by category in the mobility model of Bern, Switzerland.** Circles depict schools and research institutes (blue), social places (orange), bus stops (green), workplaces (red), supermarkets (purple).

using the following SDE with jumps:

$$dP_{i,k}(t) = dU_{i,k}(t) - dV_{i,k}(t) \tag{1}$$

where $U_{i,k}(t)$ and $V_{i,k}(t)$ are counting processes recording the events of individual i arriving at and leaving from site $k \in \mathcal{S}$, respectively. We define their dynamics as follows:

$$\begin{aligned} P\left(dU_{i,k}(t) = 1 \,|\, \mathcal{H}(t)\right) &= \lambda_{i,k}(t) \prod_{l \in \mathcal{S}} (1 - P_{i,l}(t))\, dt \\ P\left(dV_{i,k}(t) = 1 \,|\, \mathcal{H}(t)\right) &= U_{i,k}(t)\, v_k\, dt \end{aligned} \tag{2}$$

where $\lambda_{i,k}(t)$ is the rate at which individual i visits site k and $1/v_k$ is the average duration of a visit to site k. To configure the rates $\lambda_{i,k}(t)$ and average duration $1/v_k$ for every individual and site, one can resort to publicly available data. In our simulations, we use the spatial distribution of site locations, high-resolution population density data, country-specific information about household structure, and region-specific age demographics. We also assume that the probability that an individual i visits a specific site k decreases with the distance between their household and the site, similar to the gravity model [22]. Figure 1 illustrates the sites $\mathcal{S}$ in a mobility model of Bern, Switzerland, which will be used for the case study in Section 4.

2.2 Epidemiology

We build on recent variations of the Susceptible-Exposed-Infected-Resistant (SEIR) compartment models that have been introduced in the context of COVID-19 modeling [23, 24]. However, while traditional SDEs constrain the number of exposures to homogeneous Poisson distributions, we adopt a set of SDEs with jumps that employ a stochastic and dynamically adjusting exposure rate for each individual $i \in \mathcal{V}$, under which this constraint is lifted. More specifically, we define the epidemiological condition of each individual $i \in \mathcal{V}$ using the indicator state variables $\mathbb{S}(t) = \{S_i(t),\, E_i(t),\, I_i^a(t),\, I_i^p(t),\, I_i^s(t),\, H_i(t),\, R_i(t),\, D_i(t)\}_{i \in \mathcal{V}}$ with each $\in \{0, 1\}$, whose meaning is specified in Table 1. Their values and state transitions are characterized by the

Table 1: Epidemiological state variables $\mathbb{S}(t)$

State	Description	Infected	Contagious	Symptoms
$S_i(t)$	is susceptible	-	-	-
$E_i(t)$	is exposed	✓	-	-
$I_i^a(t)$	is asymptomatic, mild course of disease	✓	✓	-
$I_i^p(t)$	is pre-symptomatic, progresses to $I_i^s(t)$ later	✓	✓	-
$I_i^s(t)$	is symptomatic	✓	✓	✓
$H_i(t)$	is hospitalized	✓	✓	✓
$R_i(t)$	is resistant & recovered	-	-	-
$D_i(t)$	has died	-	-	-

following SDEs with jumps:

$$\begin{aligned}
dS_i(t) &= -S_i(t)dN_i(t) \\
dE_i(t) &= dN_i(t) - dM_i(t) \\
dI_i^a(t) &= a_i dM_i(t) - dR_i^a(t) \\
dI_i^p(t) &= (1-a_i)dM_i(t) - dW_i(t) \\
dI_i^s(t) &= dW_i(t) - (1-b_i)dR_i^s(t) - b_i dZ_i(t) \\
dR_i(t) &= a_i dR_i^a(t) + (1-a_i)dR_i^s(t) \\
dH_i(t) &= h_i I_i^s(t)dY_i(t) - (1-b_i)H_i(t)dR_i^s(t) - b_i H_i(t)dZ_i(t) \\
dD_i(t) &= b_i dZ_i(t)
\end{aligned} \tag{3}$$

where $a_i \sim \text{Bern}(\alpha_a)$ indicates whether an infected individual i is asymptomatic, $h_i \sim \text{Bern}(\alpha_h)$ whether they eventually require hospitalization, and $b_i \sim \text{Bern}(\alpha_b)$ whether they eventually die.

The counting processes $\mathbb{C}(t) = \{N_i(t),\ M_i(t),\ R_i^a(t),\ R_i^s(t),\ W_i(t),\ Y_i(t),\ Z_i(t)\}_{i\in\mathcal{V}}$ model the state transitions. For individual $i \in \mathcal{V}$, the *first* arrivals of the processes indexed by i model their transition from susceptible to exposed ($N_i(t)$), from exposed to infected ($M_i(t)$), from presymptomatic infected to symptomatic infected ($W_i(t)$), from asymptomatic infected to resistant ($R_i^a(t)$), from symptomatic infected to resistant ($R_i^s(t)$), from symptomatic infected to hospitalized ($Y_i(t)$), and from symptomatic infected to dead ($Z_i(t)$).

At the core of our modeling framework, we define the conditional intensity function $\lambda_i^*(t)$ of the exposure counting process $N_i(t)$ as

$$\lambda_i^*(t) = \sum_{k\in\mathcal{S}} \beta_k P_{i,k}(t) \sum_{j\in\mathcal{V}\setminus\{i\}} \int_{t-\delta}^{t} K_{j,k}(\tau)\ \gamma e^{-\gamma(t-\tau)}\, d\tau \tag{4}$$

where

$$K_{j,k}(\tau) = \Big(I_j^s(\tau) + I_j^p(\tau) + \mu I_j^a(\tau)\Big) P_{j,k}(\tau)$$

and $P(dN_i(t) = 1 \,|\, \mathcal{H}(t)) = \lambda_i^*(t)\, dt$. In the above:

(i) $\beta_k \geq 0$ is the transmission rate due to presymptomatic and symptomatic individuals currently visiting site k. Depending on the availability of labeled and unlabeled data, one may consider sharing the same parameter for all sites or sites of the same category.

(ii) $\mu \in [0, 1]$ is the relative transmission rate of asymptomatic compared to (pre-)symptomatic individuals.

(iii) $\int_{t-\delta}^{t} K_{j,k}(\tau)\, \gamma e^{-\gamma(t-\tau)}\, d\tau$ accounts for environmental transmission, *i.e.*, it accounts for the fact that the virus may survive for some period of time on surfaces or in the air after an infected individual has left a site [25].

The exposure intensity in (4) models that an individual's instantaneous rate of exposure increases by a constant site-specific transmission rate β_k when in contact with another infectious individual at a site $k \in \mathcal{S}$, in addition to capturing environmental transmission. Consequently, based on the mobility traces $P_{i,k}(t)$, the exposure rate of each individual i only depends on the individual's contacts at sites $k \in \mathcal{S}$, not the contacts of others. Infections within households are characterized by adding an additional analogous term $\lambda_{\mathcal{H}(i)}(t)$ with household transmission rate ξ to $\lambda_i^*(t)$, as outlined in Appendix A.

For the remaining (mobility-independent) counting processes $M_i(t)$, $R_i^a(t)$, $R_i^s(t)$, $W_i(t)$, $Y_i(t)$, and $Z_i(t)$, which characterize the state transitions after exposure, we model the times to event using log-normal distributions [26, 27] starting at the time $E_i(t)$, $I_i^p(t)$, $I_i^a(t)$ or $I_i^s(t)$ become one, respectively. Their parameters are fixed based on recent estimates by the COVID-19 literature and summarized in Table 2.

2.3 Testing

Individuals are tested according to a testing policy $\pi_{\text{test}}(t)$, *e.g.*, testing only symptomatic or vulnerable people, at a rate $\lambda_{\text{test}}(t)$, which can be chosen to match location-specific testing statistics. The test outcomes are only known after a reporting delay Δ_{test}. Formally, the counting process $T(t)$ records the number of known test outcomes by time t. Let $T_i^+(t)$ and $T_i^-(t)$ be the number of times an individual $i \in \mathcal{V}$ has been tested positive and negative, respectively, by time t. Then, we characterize the state variables $T_i^+(t)$ and $T_i^-(t)$ using the following SDEs:

$$\begin{aligned} dT_i^+(t) &= \big(E_i(t) + I_i^a(t) + I_i^p(t) + I_i^s(t)\big) d_i(t)\, dT(t + \Delta_{\text{test}}) \\ dT_i^-(t) &= \big(S_i(t) + R_i(t)\big) d_i(t)\, dT(t + \Delta_{\text{test}}) \end{aligned} \tag{5}$$

where $d_i(t) \in \{0, 1\} \sim \pi_{\text{test}}(t)$ indicates whether i is tested at time t according to the policy.

2.4 Containment measures

In the above context, we can faithfully model a variety of containment measures that not only affect the broad population $\mathcal{V}$ but also target specific sites or individuals, possibly in a time-variant fashion. These may range from less restrictive (*e.g.*, isolating individuals who have tested positive for 14 days or who had contact with a positively tested individual) to more restrictive (*e.g.*, implementing a state of "lockdown" for the entire population). The effect of mobility reduction and quarantine can be characterized by reducing the rates $\lambda_{i,k}(t)$ at which individuals visit sites in the mobility model. Hygienic measures (*e.g.*, face masks) can be implemented by reducing the transmission rate β_k at specific sites (*e.g.*, work places). In all cases, the measures reduce the conditional intensities $\lambda_i^*(t)$ of the exposure counting processes $N_i(t)$, possibly dynamically based on the values of other state variables at time t.

Moreover, if desired, we may assume that contacts between individuals at sites are registered by a peer-to-peer proximity-based tracing system, analogous to the smartphone-based Bluetooth systems that have been implemented in the context of the COVID-19 pandemic [28]. A contact between individuals i and j will be registered if (i) their visit times at a specific site $k \in \mathcal{S}$ overlap, and (ii) both opt to use the proximity-based tracing system, *e.g.*, by means of carrying a Bluetooth device. Visit times are said to overlap when $P_{i,k}(t) = 1$ and $P_{j,k}(t) = 1$ for some $k \in \mathcal{S}$ and t. When an individual i is tested positive, their registered contacts may be advised to isolate or seek testing themselves as described in Section 2.3. For contact tracing, the type of intervention may depend on the risk of exposure caused by the positively tested individual, which can be estimated using our model. Appendix B provides further details.

3 Model Simulation and Estimation

3.1 Epidemiological Sampling Algorithm

Having formally defined the model dynamics in Section 2, we now describe how to generate simulations of the individual epidemiological states $\mathbb{S}(t)$ over a time horizon $t \in [0, t_{\max}]$, which ultimately allows us to empirically study the spread of the disease under a variety of scenarios. The initial conditions $\mathbb{S}(0)$, a testing policy $\pi_{\text{test}}(t)$, and the mobility traces $P_{i,k}(t)$ are assumed to be fixed a priori—from simulations of a synthetic mobility model or real-world data.

The epidemiological state variables $\mathbb{S}(t)$ in the model SDEs (3) change at—and only change at—*events* of the counting processes $\mathbb{C}(t)$. Hence, all state variables $\mathbb{S}(t)$ are constant between two consecutive events when considering all event times of $\mathbb{C}(t)$ on *one* timeline. This leads us to the backbone principle for generating random realizations of the model: we initialize the state variables $\mathbb{S}(0)$, sample the next time of state transition for each $i \in \mathcal{V}$, and push these transition events onto *one* single temporally-sorted priority queue Q, simultaneously tracking the next events for *all* individuals in the model. The algorithm then repeatedly loops through: (i) popping the next event e from Q; (ii) updating the state of individual i associated with e; (iii) sampling the next time t of state transition e' for i; and (iv) pushing e' to Q with priority t.

As explained in Section 2, we fix the time-to-event distributions of all non-exposure processes $\mathbb{C}(t)\backslash\{N_i(t)\}_{i\in\mathcal{V}}$ to independent, easy-to-sample distributions as estimated by clinical COVID-19 literature. Thus, sampling the first event time of $N_i(t)$ (the time of exposure of i) is the central difficulty, with rate $\lambda_i^*(t)$ dynamically interacting with all other stochastic state variables $\mathbb{S}(t)$ via the mobility model $P_{i,k}(t)$. To this end, we first decompose the intensity $\lambda_i^*(t)$ into a sum of contributions $\lambda_{j\to i}^*(t)$ caused by other individuals j:

$$\lambda_i^*(t) = \sum_{j\in\mathcal{V}\backslash\{i\}} \sum_{k\in\mathcal{S}} \beta_k P_{i,k}(t) \int_{t-\delta}^{t} K_{j,k}(\tau)\gamma e^{-\gamma(t-\tau)}\, d\tau \quad =: \sum_{j\in\mathcal{V}\backslash\{i\}} \lambda_{j\to i}^*(t) \tag{6}$$

where the last summation over $j \in \mathcal{V}\backslash\{i\}$ is sparse as it only indexes over contacts of individuals i after time t. Note that $\lambda_{j\to i}^*(t) = 0$ when i and j are not in contact directly or when j left site $k \in \mathcal{S}$ more than δ-time before i arrived.

By (6), the counting process $N_i(t)$ can be seen as a superposition of several processes $N_{j\to i}(t)$ with intensities $\lambda_{j\to i}^*(t)$. More precisely, the time-to-event distribution of $N_i(t)$ is equivalent to the distribution of the time to the *first* arrival of all processes $N_{j\to i}(t)$ [21, 29]. Hence, using the temporal ordering invariant of Q, we can process valid exposure events on the fly. Whenever an individual j becomes infectious—either via $I_j^a = 1$ or $I_j^p = 1$—we sample the next exposure event that j *causes* for every individual i in contact with j in the future at rate $\lambda_{j\to i}^*(t)$, and push these events onto Q. When an exposure event e for individual i is popped from Q in step (i), we check that e is the *first* exposure of i by verifying $S_i(t) = 0$, and discard later exposure events for i. The next event time of $N_{j\to i}(t)$ after time t' is sampled using thinning [21], *i.e.*, by adding up $\tau \sim \text{Expo}(\lambda_{j\to i}^{\max})$ to t' until stopping with probability $\lambda_{j\to i}^*(t')/\lambda_{j\to i}^{\max}$, where $\lambda_{j\to i}^{\max}$ is an upper bound on $\lambda_{j\to i}^*(t)$. We skip zero-intensity windows whenever reaching $\lambda_{j\to i}^*(t) = 0$ during thinning, which is sound by viewing $N_{j\to i}(t)$ itself as a superposition of counting processes, one for each interval of non-zero intensity, and skipping their initial zero-rate periods by the memoryless property.[3]

If j recovers, i.e. $R_j(t) = 1$, then $\lambda_{j\to i}^*(t)$ in (6) is dynamically set to 0 at the time of recovery. By the principle of thinning, all exposure events caused by j beyond this point—sampled back when j got infectious—are discarded on the fly, *i.e.*, when they get popped from Q. Lastly, note that interventions like social distancing or hygienic measures always *reduce* the rates $\lambda_{j\to i}^*(t)$ and can thus likewise be implemented using thinning, *i.e.*, rejecting the affected exposure events with some probability.

Combining the above, we arrive at an efficient sampling procedure for the epidemiological model SDEs using a single priority queue Q, which is formally provided in Algorithms 2 and 3 of the Appendix. While a formal analysis of its computational complexity depends on many moving parts, we have empirically found that the algorithm scales to regions of at least one hundred thousand inhabitants. Moreover, note that random simulation rollouts of the model can be embarrassingly parallelized.

[3] If $T \sim \text{Expo}(\lambda)$, then $P(T \geq t + s \mid T \geq s) = P(T \geq t)$.

Algorithm 1 Parameter estimation using Bayesian optimization

Input: Black-box simulator $g_t(\theta)$, parameter domain $\mathrm{dom}(\theta)$, time horizon $t_{\max}$, case data c_t^{true}, hyperparameters J, M, N

$s(\mathbf{x}) := -\sum_{t=1}^{t_{\max}} (c_t^{\text{true}} - \mathbf{x}_t)^2$
$\theta_{1:M} \leftarrow$ first M quasi-random settings
$\mathcal{D} \leftarrow \emptyset$
for $i \in [M]$ **do** ▷ Quasi-random initialization
    Obtain daily sim. result $g_t(\theta_i)$ from J random roll-outs
    $\mathcal{D} \leftarrow \mathcal{D} \cup \{(\theta_i, g_t(\theta_i))\}$
while $|\mathcal{D}| \leq N$ **do** ▷ Bayesian Optimization
    $p(g_t(\theta)) \mid \mathcal{D}) \leftarrow$ GaussianProcessPosterior($\mathcal{D}$)
    $\theta^* \leftarrow \arg\max_{\theta' \in \mathrm{dom}(\theta)} \mathrm{KnowledgeGradient}(p, \theta')$ [33]
    Obtain daily sim. result $g_t(\theta^*)$ from J random roll-outs
    $\mathcal{D} \leftarrow \mathcal{D} \cup \{(\theta^*, g_t(\theta^*))\}$
return $\arg\max_{(\theta, g_{1:t_{\max}}(\theta)) \in \mathcal{D}} \; s(g_{1:t_{\max}}(\theta))$

3.2 Parameter Estimation

Building on the sampling algorithm, we are able to estimate the exposure-related epidemiological parameters $\theta = \{\beta_k, \xi\}$, *i.e.*, the transmission rate of individuals at sites and in their households, in a given epidemiological scenario. More specifically, provided a set of initial conditions $\mathbb{S}(0)$, a testing policy π_{test}, a priori fixed mobility traces $P_{i,k}(t)$, and fixed parameters of the non-exposure processes $\mathbb{C}(t) \backslash \{N_i(t)\}_{i \in \mathcal{V}}$, we can estimate the parameters θ that provide the best fit to the observed COVID-19 cases in a given region. To this end, we view the model simulation as a black box and apply Bayesian optimization (BO), which amounts to iteratively building a surrogate model of the fitting objective and evaluating at promising parameter settings [17].

Following the standard BO paradigm, we interpret the *expected number of positive cases at time t* in our model as a black box function $g_t(\theta)$ where

$$g_t(\theta) := \mathbb{E}_{\mathcal{T} \sim \theta} \Big[\sum_{T_i^+ \in \mathcal{T}} T_i^+(t) \Big] \tag{7}$$

The expectation in (7) is defined over realizations of the testing state variables $\{T_i^+(t)\} =: \mathcal{T} \sim \theta$ of the model with exposure parameters θ. In practice, $g_t(\theta)$ is only observed via noisy evaluations at different values of θ since the expectation is approximated using a Monte Carlo estimate of J random simulations. $\mathcal{T}$ is stochastic not only due to the counting processes, but in absence of real mobility traces also due to random seeds $\mathbb{S}(0)$ and synthetic $P_{i,k}(t)$, independently simulated for each rollout.

The objective we aim to minimize is the *mean daily squared error* of cumulative positive cases between the model predictions and the real observed COVID-19 cases of the region. This allows us to form a link between the spatiotemporal states of each individual in the model and aggregate longitudinal case data. The squared error has previously been considered in parameter estimation for black-box models [30] and in the context of COVID-19 research [31]. Let c_t^{true} be the cumulative number of real COVID-19 cases at the end of day t as provided by the national authorities. Then, our objective f to be minimized is a composition of the squared error score and per-day black-box functions $g_t(\theta)$ averaged over a time of $t_{\max}$ days:

$$f(\theta) = \frac{1}{T} \sum_{t=1}^{t_{\max}} \Big(c_t^{\text{true}} - g_t(\theta) \Big)^2 \tag{8}$$

The compositionality of f can allow for greater sample efficiency [30, 32], in particular when estimating additional parameters. However, when only estimating $\theta = \{\{\beta_k\}, \xi\}$ and β_k held constant across sites, we found it to be favorable for the BO surrogate model to directly learn $f(\theta)$, as opposed to the daily $g_t(\theta)$, as the black-box function. We use the knowledge gradient acquisition function [33] to navigate parameter proposals, which often shows favorable performance in noisy settings [32, 34]. Combining the above into the BO paradigm, the parameter estimation procedure is summarized in Algorithm 1.

4 A Case Study of Bern, Switzerland

4.1 Experimental Setup

We showcase the flexibility of our modeling framework in a case study of the city of Bern, Switzerland. By leveraging fine-grained demographic data and open-source site locations, we build a mobility model of the city that contains $|\mathcal{V}| = 133{,}790$ individual inhabitants that visit $|\mathcal{S}| = 2{,}174$ real points of interest. Using this mobility model, we then estimate both a constant transmission rate at sites β and in households ξ using the procedure described in Section 3. To this end, we use longitudinal COVID-19 case data from early in the pandemic. Finally, we simulate and study the course of the COVID-19 epidemic under various containment measures (Sections 2.3-2.4).

Mobility traces In the mobility model of Bern, individuals $\mathcal{V}$ belong to one of nine age groups according to the real demographics of the region. These individuals are placed in households of up to five people according to their age and reported household structure in Switzerland [35]. The households themselves are located across the spatial expansion of the city using high-resolution population density data provided by *Facebook Data for Good* [36]. To obtain relevant site locations in the regions of interest, we use geolocation data provided by *OpenStreetMap* [37]. Specifically, we retrieve the location of all sites $\mathcal{S}$ in five site categories: *education* (schools, universities, research institutes), *social* (restaurants, cafés, bars), *transportation* (bus stops), *work* (offices, shops), and *groceries* (supermarkets, convenience stores). The sites $\mathcal{S}$ are visualized in Figure 1.

For lack of available real check-in traces $P_{i,k}(t)$, we simulate synthetic mobility traces under assumption of the gravity model [22]. In particular, we assume that each individual $i \in \mathcal{V}$ visits only a constrained set of unique sites $\mathcal{S}_i \subset \mathcal{S}$, which are selected with probability inversely proportional to the squared distance from their homes. This reflects the fact that individuals typically study or work at only one place, form habits regarding the public transportation they use, and social places or supermarkets they visit. We set the check-in rate $\lambda_{i,k}(t)$ of Section 2.1 to a constant value that depends on the individual's age group and site type; see Table 3 in the Appendix. The mean duration $1/\nu_k$ at sites of type education and work, social, transportation, and groceries are fixed to 120, 90, 12 and 30 minutes, respectively. These times are sometimes set to lower values than one would expect because individuals are neither exposed to all others at a site nor continuously exposed during their visit.

Estimation of transmission rate parameters To estimate the transmission rate at sites β and in households ξ, we run the procedure described in Section 3.2 for at least $N > 100$ steps with $M = 10$ initial quasi-random settings and $J = 200$ rollouts. We use COVID-19 case data of county-level administrative regions [38] to define the objective (8) and set mortality and hospitalization rates per age group using this data and previous studies [39]. We consider the time horizon from early March 2020 until May 2020 as the estimation window since it includes both times before and during governmental interventions in Switzerland, which occurred largely from March 16, 2020 to May 10, 2020 [40]. During governmental interventions, the check-in frequencies of individuals at sites in the mobility model are reduced as estimated by Google mobility data in the region [41], and education and social sites are closed, *i.e.*, not visited at all. In the model simulations used for estimation, each of the J realizations is randomized across realizations of the synthetic mobility traces and infection seeds. Initially exposed and infectious individuals are heuristically selected as described in Appendix C based on knowledge about the case numbers at the start date of the estimation period.

Testing To abstract away from testing criteria implemented in different regions, we assume that only true symptomatic individuals are registered for testing and that tests have perfect accuracy. We set the reporting delay Δ_{test} to 30 minutes, accounting for the now frequently available[4] rapid tests [42], and assume that there is sufficient capacity to test all selected individuals. Moreover, positively tested individuals and their household members are quarantined for 14 days in isolation from each other.

[4]During parameter estimation, Δ_{test} is set to 48 hours to account for the test delay early in the pandemic.

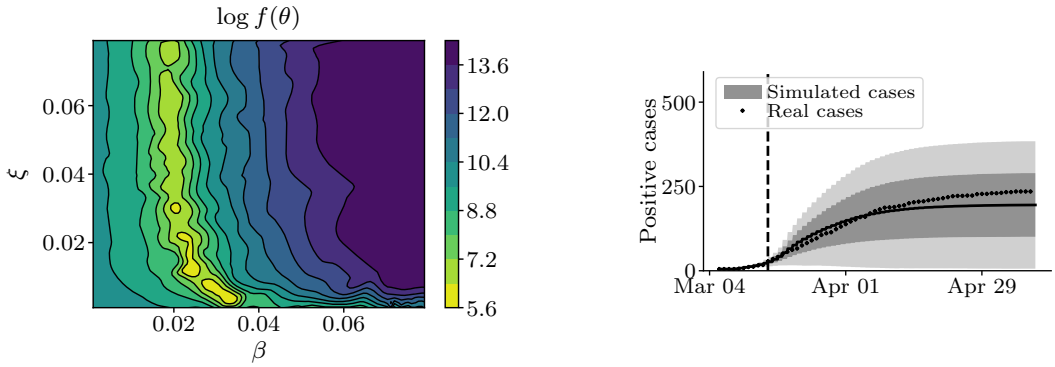

Figure 2: **Transmission parameter estimation for the model of Bern, Switzerland**. The left plot shows a contour plot of the log objective in (8) as a function of the transmission rate at sites β and in households ξ. The estimated parameters $\beta = 0.0337$ and $\xi = 0.0038$ lie in the identifiable optimal region. The right plot shows the predicted and real cumulative cases under the estimated parameters. The "lockdown" measures in Switzerland were implemented on March 16, 2020 as indicated by the dashed vertical line. The solid line indicates the mean, the shaded areas one and two standard deviations across 100 random simulations, respectively.

4.2 Model Fit and Parameter Estimation

Figure 2 visualizes both the objective values $f(\boldsymbol{\theta})$ obtained at various settings for the transmission rates β and ξ as well as the model predictions for the cumulative cases during the time window of parameter estimation. The contour plot indicates that there is a single and identifiable optimal parameter regime, whose optimal values were estimated as $\beta = 0.0337$ and $\xi = 0.0038$. Furthermore, we find that the simulations using the estimated parameters are able to accurately match the observed longitudinal trend of cases during the estimation period early in the epidemic. Appendix D provides a collection of parameter estimation results for four additional regional models of other urban and rural regions in Switzerland and Germany [43–45]. These supplementary findings confirm a similarly identifiable optimal parameter regime and demonstrate that both the epidemiological model and the transmission parameter estimation procedure are robustly applicable to other regional mobility models.

In the remainder of this section, we use the estimated transmission parameters for the model of Bern in all of our experiments. We first empirically validate that, under our mobility and fitted transmission model, the number of secondary infections caused by infectious individuals is overdispersed. Finally, we use our framework to quantify the effects of a range of containment measures. To create a general epidemiological scenario, we assume a small but continual influx of five untraceable exogenous exposures per 100,000 inhabitants and per week and simulate the model state variables over a period of four months.

4.3 Overdispersion of Secondary Infections

As argued in Section 1, existing epidemiological models have predominantly built on homogeneous Poisson transmission dynamics that fail to capture the overdispersion of secondary infections observed for COVID-19. In addition, they do not explicitly model visits to sites where exposures occur. As a result, these models have been of little use for studying and predicting where and when infection hotspots are most likely to occur [6, 10, 12, 16].

In contrast, we find that, under our model, overdispersion of secondary infections can emerge naturally. More specifically, we simulate the spread of COVID-19 under no containment measures other than the testing of symptomatic and isolation of positively tested individuals. During these simulations, we count the number of secondary infections caused by individuals that got infectious during during a 7-day window after 1 month of the model simulations. Using two goodness-of-fit tests for the Poisson distribution, the Chi-squared (χ^2)

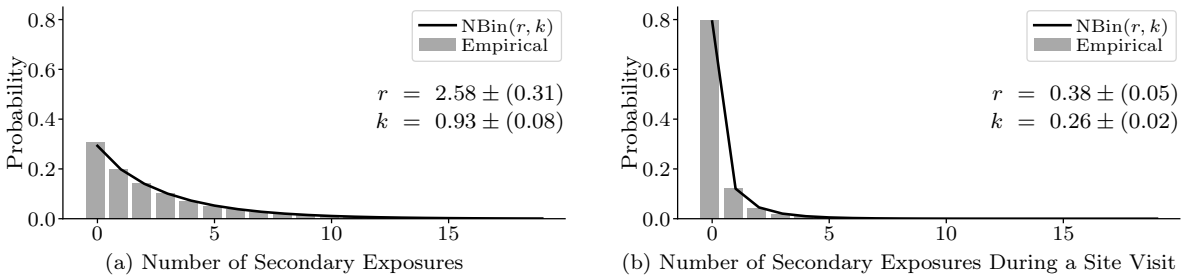

(a) Number of Secondary Exposures (b) Number of Secondary Exposures During a Site Visit

Figure 3: **Overdispersion of Secondary Infections.** Panels a) and b) show a generalized negative binomial model fitted by maximum likelihood estimation to the secondary infections caused by an infectious individual, overall and stratified by site visits, respectively, and averaged over 100 random realizations. The secondary infections are counted for individuals that got infectious during a 7-day window after 1 month of the simulation under no containment measures other than the testing of symptomatic and isolation of positively tested individuals.

and variance tests (VT) [46, 47], we are able to reject the null hypothesis that the distribution of secondary infections, both overall and when stratified per visit, follows a Poisson distribution. In particular, for both distributions of secondary infections, we obtain $p_{\chi^2} < 10^{-8}$ and $p_{\mathrm{VT}} < 10^{-8}$. With sample variance generally significantly exceeding the sample mean, both ways of counting the number of secondary infections naturally exhibit a higher variance than expected under the Poisson assumption and are thus *overdispersed*.

Building on this result, we follow recent work in the context of COVID-19 [4, 7] and measure the degree of overdispersion by fitting a generalized negative binomial distribution $\mathrm{NBin}(r, k)$, an overdispersed generalization of the Poisson, where $r > 0$ is the mean or reproduction number, and k is the dispersion parameter. Figure 3 summarizes the results. Averaged over 100 random realizations, we find that the dispersion parameter $k < 1$ both overall and when stratified per visit ($k = 0.93 \pm (0.08)$ and $k = 0.26 \pm (0.02)$, respectively), evidence of substantial overdispersion [4]. We hypothesize that the higher overdispersion observed when aggregating per visit is a direct effect of the interaction between the stochastic check-in mobility model and our model of transmission at sites.

4.4 Efficacy of containment measures

Reducing contacts at public sites by restricting individual mobility has been one of the most prevalent measures to counteract the spread of COVID-19 [48]. Our modeling framework allows us to faithfully study how effective various variants of this approach are at, *e.g.*, containing the disease, reducing peak hospitalizations, or changing the effective reproduction number R_t over time. Instead of restricting the mobility of the entire population or only vulnerable groups, previous work has, for instance, proposed to divide the population into two subgroups that get isolated on alternating days [49, 50].

Figure 4 shows a comparative analysis of three of these variants: restricting the mobility of everyone, only vulnerable groups, or one of two random subgroups on alternating days. For each variant, we consider different levels of mobility restriction where individual check-in activity at sites in the mobility model is reduced by between 5% and 75%. In our simulations, the vulnerable groups are defined as individuals older than 60 years, who typically suffer more complications from COVID-19 [38, 43]. Our findings highlight the fact that the efficacy of each policy strongly depends on the degree to which individual movement activity is reduced. While restricting the mobility of everyone is overall clearly most effective, our findings suggest that isolating (i.e., reducing the mobility by 100%) one of two subgroups on alternating days can reduce the effective reproduction number, averaged over the phase of exponential case growth, and peak hospitalizations as much as reducing the mobility of everyone by 50%. Moreover, our results also suggest that the morally debatable strategy of quarantining only vulnerable groups does not live up to its expectation of reducing peak hospitalizations significantly.

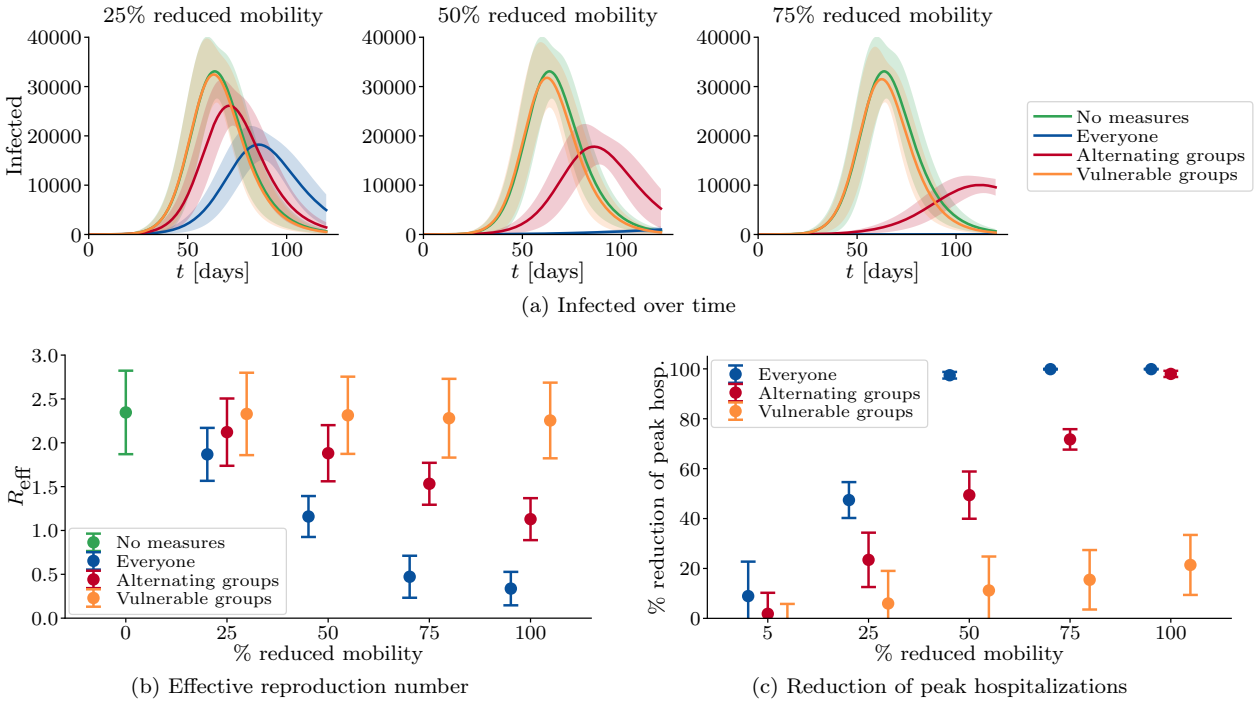

(a) Infected over time

(b) Effective reproduction number

(c) Reduction of peak hospitalizations

Figure 4: **Mobility restrictions.** Individuals of certain groups reduce their mobility, i.e., their frequency of visits to sites by a certain proportion. Panel a) shows the number of infected over time for different levels of mobility restrictions. Panel b) shows the effective reproduction number during the phase of exponential growth of the number of infected. Panel c) shows the reduction of peak hospitalizations compared to a scenario without mobility restrictions. Points and lines represent the mean over 100 rollouts of the simulation. Error bars and shaded regions correspond to plus and minus one and two standard deviations respectively.

Orthogonal to various strategies that aim at reducing the number of contacts, the promise of digital contact tracing has been to achieve fine-grained epidemic control without severe societal or economical restrictions [24]. In this section, whenever an individual is tested positive, we use contact tracing to identify all of their contacts in the 10 days leading up to the test result (see Section 2.4). If a given contact was longer than 15 minutes—the time threshold used by the national COVID-19 tracing apps in, *e.g.*, France, Germany, Switzerland, and the United Kingdom [51–54]—the contact person is tested and isolated from everyone in the mobility model for 14 days.

We analyze the effectiveness of digital contact tracing in combination with various degrees of mobility restrictions for the entire population at different digital tracing adoption levels. The findings shown in Figure 5a illustrate that the adoption of the digital tracing system and the activity reduction due to social distancing have a complementary relationship in reducing the cumulative number of infections, as already argued by previous work [55]. Furthermore, the results suggest that, while contact tracing can provide a significant contribution to the mitigation of an epidemic, even at high adoption levels of 75%, it requires combination with activity reductions of 25% and above in order to achieve epidemic control ($R_t < 1$). The effective reproduction number R_t shown in Figure 5b decreases over time at a constant adoption level due to the growing number of recovered individuals in the population.

5 Related Work

Our work builds upon previous work on compartmental epidemiological modeling, human mobility models, and temporal point processes. Most of the classical epidemiological literature has focused on developing

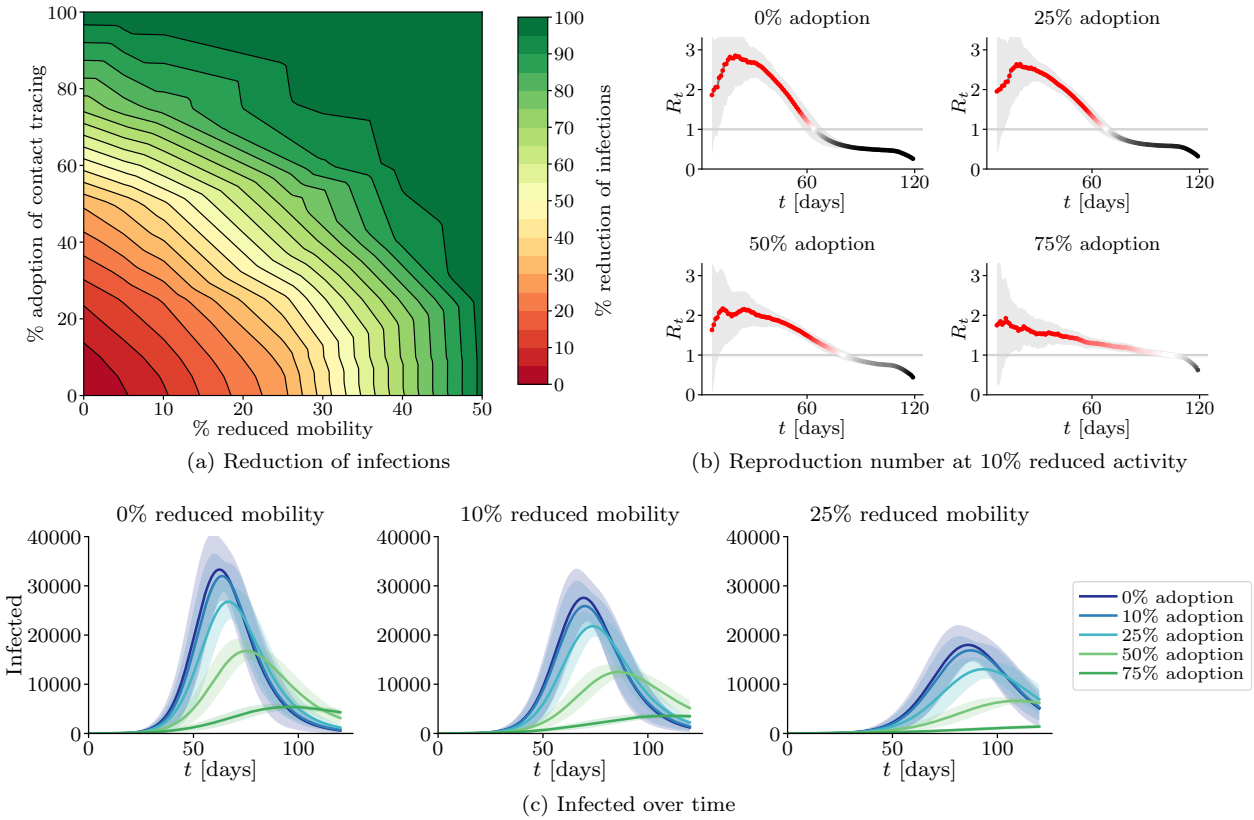

Figure 5: **Contact tracing.** A certain proportion of the population has adopted a digital contact tracing system and, in addition, everyone reduces their visit frequency to sites by a certain proportion. Quarantine measures are imposed on traceable individuals who have been in contact with positively tested individuals for a minimum of 15 minutes. Panel a) shows the reduction of the cumulative number of infections compared to a scenario without interventional measures for different adoption levels of the tracing technology and various degrees of mobility restrictions. Panel b) shows the reproduction number over time for different adoption levels at a fixed mobility reduction of 10%. Panel c) shows the number of infected individuals over time for different scenarios. Lines and shaded regions represent the mean and two standard deviations computed over 100 rollouts of the simulation respectively.

population models [56], unable to capture heterogeneous transmission dynamics at the individual level. More recently, there has been research on agent-based epidemic modeling [57–61], also in the context of COVID-19 [23, 39, 62–66]. These models predominantly use multi-layer contact networks, discrete time, metapopulation, or Poisson transmission rate assumptions to characterize individual infections, rather than the frequency and duration of each individual's visits to specific sites, as our model does. Notable exceptions are by Aleta et al. [67], who use check-in data of real sites, yet only to configure the layers of a multi-layer contact network, and Ferreti et al. [24], who employ a time-varying transmission rate, but average over individuals who infect few or many others. Chang et al. [31] consider specific points of interest in US cities but only model transmission dynamics of metapopulations of up to 3,000 people rather than among single individuals. Ultimately, none of the above models, including these three exceptions, can be faithfully used to characterize the dispersion of the number of individual infections during a visit, or to straightforwardly study the course of a disease under fine-grained intervention policies such as, *e.g.*, contact tracing or COVID-19 testing.

The literature on human mobility models has a rich history, which has been extensively reviewed by Barcosa et al. [68]. In our experiments, the spatial distribution of visits of our *event-based* "check-in" mobility

model follows the gravity model [22]. Analogous to previous COVID-19 research, these visits are synthetically generated in each simulation [49, 69, 70]. However, our formulation is not restricted to this specific choice and one could think of designing event-based mobility models with a spatial distribution of visits following, *e.g.*, the radiation model [71] or population-weighted opportunities model [72]. That said, the configuration of visit types, frequencies, and durations are specific to event-based models as ours, where the existing body of work on mobility models provides only very limited guidance [73, 74].

Finally, there has been a flurry of work on temporal point process modeling in the machine learning literature in recent years [75–78]. They have been particularly successful in predicting information propagation in social networks and the web, where they have achieved state of the art performances [79, 80]. However, the development of compartmental epidemiological models based on temporal point processes has been lacking.

6 Discussion

Motivated by multiple lines of evidence that strongly suggest for infection hotspots to play a key role in the transmission dynamics of COVID-19, we have introduced a spatiotemporal epidemic model that explicitly represents sites where infections occur and hotspots may emerge. Through a case study that used fine-grained demographic data, site locations, mobility data, as well as COVID-19 case data from Bern, Switzerland, we have demonstrated that our model can allow individuals and policy-makers to make more effective decisions concerning the implementation of containment measures, contact tracing, and testing at the individual level. To facilitate this, we have released an easy-to-use implementation of the entire framework necessary to perform experiments for any desired region [20]. While the purpose of this work does not lie in providing mechanistic forecasts, we have shown that an identifiable pair of only two fitted parameters, the transmission rates at sites and in households, provides reasonable predictiveness over our estimation window. Importantly, our epidemiological model empirically exhibits overdispersion in the number of secondary infections, suggesting that our formulation characterizes the transmission dynamics at infection hotspots—an epidemiological driver that effective containment measures would demand preventing [10, 16].

Finally, in this work, we have used fine-grained demographic data and site locations to configure our mobility model. However, if contact tracing data become accessible to researchers, we believe that the variance of our predictions could be lowered and that it would be possible to use our framework to identify areas with higher risk of infection in real time. Beyond legal compliance and gaining societal acceptance, the use of epidemic models with high spatiotemporal resolution such as ours should respect each individual's privacy. In this context, it is important to highlight that, both during parameter estimation and contact tracing, we only need to compute the contact *duration* of individuals with an infected person—the identity of the infected person is not required. As a result, there are reasons to believe that such computations can be made in a decentralized and privacy-preserving manner [81, 82]. Ultimately, although our model has greater resolution than many of those in use today, its predictions can only be faithfully considered when being aware of the high variance observed across random realizations.

Acknowledgements

We thank the Robert-Koch-Institute, OpenStreetMaps, Google, and Facebook for providing data to make this work possible. We thank Brian Karrer from Facebook for his insightful comments and suggestions regarding Bayesian optimization, Kevin Murphy, Yusef Shafi and others from Google for helpful discussions, and Yannik Schaelte for useful comments on a preliminary version of this work. We thank Cansu Culha and the Stanford Future Bay Initiative as well as Pavol Harar from the University of Vienna for working with us to improve our publicly available implementation. This work was supported in part by SNSF under grant number 200021-182407 and the European Research Council (ERC) under the European Union's Horizon 2020 research and innovation programme (grant agreement No. 945719).

References

[1] Johns Hopkins University & Medicine: coronavirus resource center. https://coronavirus.jhu.edu/ (2020).

[2] Adam, D. C. *et al.* Clustering and superspreading potential of SARS-CoV-2 infections in hong kong. *Nature Medicine* **26**, 1714–1719 (2020).

[3] MSF. Too little, too late: The unacceptable neglect of the elderly in care homes during the COVID-19 epidemic in spain (2020).

[4] Endo, A. *et al.* Estimating the overdispersion in COVID-19 transmission using outbreak sizes outside china. *Wellcome Open Research* **5** (2020).

[5] Lau, M. S. *et al.* Characterizing superspreading events and age-specific infectiousness of SARS-CoV-2 transmission in georgia, usa. *Proceedings of the National Academy of Sciences* **117**, 22430–22435 (2020).

[6] Frieden, T. & Lee, C. Identifying and interrupting superspreading events—implications for control of severe acute respiratory syndrome coronavirus 2 (2020).

[7] Athreya, S., Gadhiwala, N. & Mishra, A. Effective reproduction number and dispersion under contact tracing and lockdown on COVID-19 in karnataka. *medRxiv* (2020).

[8] The Korean clusters: How coronavirus cases exploded in south korean churches and hospitals. https://graphics.reuters.com/CHINA-HEALTH-SOUTHKOREA-CLUSTERS/0100B5G33SB/index.html (2020).

[9] Walker, A. *et al.* Genetic structure of SARS-CoV-2 reflects clonal superspreading and multiple independent introduction events, north-rhine westphalia, germany, february and march 2020. *Eurosurveillance* **25**, 2000746 (2020).

[10] Cevik, M., Marcus, J., Buckee, C. & Smith, T. SARS-CoV-2 transmission dynamics should inform policy. *SSRN 3692807* (2020).

[11] Hasan, A. *et al.* Superspreading in early transmissions of COVID-19 in indonesia. *Scientific reports* **10**, 1–4 (2020).

[12] Zhang, Y., Li, Y., Wang, L., Li, M. & Zhou, X. Evaluating transmission heterogeneity and super-spreading event of COVID-19 in a metropolis of china. *International journal of environmental research and public health* **17**, 3705 (2020).

[13] Oh, M.-d. *et al.* Middle east respiratory syndrome coronavirus superspreading event involving 81 persons, korea 2015. *Journal of Korean medical science* **30**, 1701 (2015).

[14] Lloyd-Smith, J. O., Schreiber, S. J., Kopp, P. E. & Getz, W. M. Superspreading and the effect of individual variation on disease emergence. *Nature* **438**, 355–359 (2005).

[15] Stein, R. A. Super-spreaders in infectious diseases. *International Journal of Infectious Diseases* **15**, e510–e513 (2011).

[16] Althouse, B. M. *et al.* Stochasticity and heterogeneity in the transmission dynamics of SARS-CoV-2. *arXiv preprint arXiv:2005.13689* (2020).

[17] Brochu, E., Cora, V. M. & de Freitas, N. A tutorial on bayesian optimization of expensive cost functions, with application to active user modeling and hierarchical reinforcement learning (2010). 1012.2599.

[18] Jones, D. R., Schonlau, M. & Welch, W. J. Efficient global optimization of expensive black-box functions. *Journal of Global optimization* **13**, 455–492 (1998).

[19] Snoek, J., Larochelle, H. & Adams, R. P. Practical bayesian optimization of machine learning algorithms 2951–2959 (2012).

[20] Lorch, L. *et al.* Data and code from "Quantifying the Effects of Contact Tracing, Testing, and Containment Measures in the Presence of Infection Hotspots". https://github.com/covid19-model/simulator (2020).

[21] De, A., Upadhyay, U. & Gomez-Rodriguez, M. Temporal point processes. Tech. Rep., Technical report, Saarland University (2019).

[22] Zipf, G. K. The P 1 P 2/D hypothesis: on the intercity movement of persons. *American sociological review* **11**, 677–686 (1946).

[23] Li, R. *et al.* Substantial undocumented infection facilitates the rapid dissemination of novel coronavirus (SARS-CoV-2). *Science* **368**, 489–493 (2020).

[24] Ferretti, L. *et al.* Quantifying SARS-CoV-2 transmission suggests epidemic control with digital contact tracing. *Science* **368** (2020).

[25] Van Doremalen, N. *et al.* Aerosol and surface stability of SARS-CoV-2 as compared with SARS-CoV-1. *New England journal of medicine* **382**, 1564–1567 (2020).

[26] Lauer, S. A. *et al.* The incubation period of coronavirus disease 2019 (COVID-19) from publicly reported confirmed cases: estimation and application. *Annals of internal medicine* **172**, 577–582 (2020).

[27] Linton, N. M. *et al.* Incubation period and other epidemiological characteristics of 2019 novel coronavirus infections with right truncation: a statistical analysis of publicly available case data. *Journal of clinical medicine* **9**, 538 (2020).

[28] Ahmed, N. *et al.* A survey of COVID-19 contact tracing apps. *IEEE Access* **8**, 134577–134601 (2020).

[29] Aalen, O. O., Borgan, Ø. & Gjessing, H. K. *Survival and Event History Analysis* (Springer New York, 2008).

[30] Astudillo, R. & Frazier, P. I. Bayesian optimization of composite functions (2019). 1906.01537.

[31] Chang, S. *et al.* Mobility network models of COVID-19 explain inequities and inform reopening. *Nature* **589**, 82–87 (2021).

[32] Balandat, M. *et al.* Botorch: Programmable bayesian optimization in pytorch (2019). 1910.06403.

[33] Wu, J. & Frazier, P. The parallel knowledge gradient method for batch bayesian optimization. In *Advances in Neural Information Processing Systems 29*, 3126–3134 (Curran Associates, Inc., 2016).

[34] Frazier, P. I. A tutorial on bayesian optimization (2018). 1807.02811.

[35] Bundesamt für Statistik, Schweiz. Households. https://www.bfs.admin.ch/bfs/de/home/statistiken/bevoelkerung/stand-entwicklung/haushalte.html (2020).

[36] Facebook Data for Good. https://dataforgood.fb.com (2020).

[37] OpenStreetMap. https://www.openstreetmap.org/ (2020).

[38] Bundesamt für Gesundheit, Schweiz. BAG COVID19 situation summary. https://www.bag.admin.ch/bag/en/home/krankheiten/ausbrueche-epidemien-pandemien/aktuelle-ausbrueche-epidemien/novel-cov/situation-schweiz-und-international.html (2020).

[39] Ferguson, N. M. *et al.* Impact of non-pharmaceutical interventions (npis) to reduce COVID-19 mortality and healthcare demand. imperial college COVID-19 response team. *Imperial College COVID-19 Response Team* 20 (2020).

[40] Der Schweizerische Bundesrat. Verordnung 2 über Massnahmen zur Bekämpfung des Coronavirus (COVID-19) (COVID-19-Verordnung 2). https://www.admin.ch/opc/de/classified-compilation/20200744/index.html (2020).

[41] Google. COVID-19 community mobility reports. https://www.google.com/covid19/mobility/ (2021).

[42] European Center for Disease Prevention and Control. An overview of the rapid test situation for COVID-19 diagnosis in the eu/eea. https://www.ecdc.europa.eu/sites/default/files/documents/Overview-rapid-test-situation-for-{COVID-19}-diagnosis-EU-EEA.pdf (2020).

[43] Robert Koch-Institut (RKI). COVID19 data set. https://npgeo-corona-npgeo-de.hub.arcgis.com/datasets/ (2020).

[44] Land Baden-Württemberg. Verordnung der Landesregierung über infektionsschützende Massnahmen gegen die Ausbreitung des Virus SARS-Cov-2 (Corona-Verordnung). https://www.baden-wuerttemberg.de/de/service/aktuelle-infos-zu-corona/aktuelle-corona-verordnung-des-landes-baden-wuerttemberg/ (2020).

[45] Bundesländer der Bundesrepublik Deutschland. Corona-Regelungen in den Bundesländern. https://www.bundesregierung.de/breg-de/themen/coronavirus/corona-bundeslaender-1745198 (2020).

[46] Cochran, W. G. Some methods for strengthening the common χ 2 tests. *Biometrics* **10**, 417–451 (1954).

[47] Fisher, R. A. Statistical methods for research workers. In *Breakthroughs in statistics*, 66–70 (Springer, 1992).

[48] Islam, N. *et al.* Physical distancing interventions and incidence of coronavirus disease 2019: natural experiment in 149 countries. *bmj* **370** (2020).

[49] Karin, O. *et al.* Adaptive cyclic exit strategies from lockdown to suppress COVID-19 and allow economic activity. *MedRxiv* (2020).

[50] Meidan, D., Cohen, R., Haber, S. & Barzel, B. An alternating lock-down strategy for sustainable mitigation of COVID-19. *arXiv preprint arXiv:2004.01453* (2020).

[51] Ministre des Solidarites et de la Sante. TousAntiCovid : responses a vos questions. https://solidarites-sante.gouv.fr/soins-et-maladies/maladies/maladies-infectieuses/coronavirus/tousanticovid.

[52] Corona-Warn-App Team. Corona-Warn-App: Documentation. https://github.com/corona-warn-app/cwa-documentation/.

[53] United Kingdom National Health Service. NHS COVID-19 app risk-scoring algorithm. https://covid19.nhs.uk/risk-scoring-algorithm.html.

[54] Federal Office of Public Health, Switzerland. How the SwissCovid app issues warnings. https://www.bag.admin.ch/bag/en/home/krankheiten/ausbrueche-epidemien-pandemien/aktuelle-ausbrueche-epidemien/novel-cov/swisscovid-app-und-contact-tracing.html#-1674020142.

[55] Contreras, S. *et al.* The challenges of containing SARS-CoV-2 via test-trace-and-isolate. *Nature communications* **12**, 1–13 (2021).

[56] Hethcote, H. W. The mathematics of infectious diseases. *SIAM review* **42**, 599–653 (2000).

[57] Ahn, H. J. & Hassibi, B. Global dynamics of epidemic spread over complex networks. In *CDC* (2013).

[58] Cator, E. & Van Mieghem, P. Second-order mean-field susceptible-infected-susceptible epidemic threshold. *Physical review E* (2012).

[59] Chakrabarti, D., Wang, Y., Wang, C., Leskovec, J. & Faloutsos, C. Epidemic thresholds in real networks. *ACM Transactions on Information and System Security (TISSEC)* **10**, 1–26 (2008).

[60] Van Mieghem, P. The N-intertwined SIS epidemic network model. *Computing* (2011).

[61] Van Mieghem, P., Omic, J. & Kooij, R. Virus spread in networks. *IEEE/ACM TON* (2009).

[62] Moghadas, S. M. *et al.* Projecting hospital utilization during the COVID-19 outbreaks in the united states. *Proceedings of the National Academy of Sciences* **117**, 9122–9126 (2020).

[63] Wells, C. R. *et al.* Impact of international travel and border control measures on the global spread of the novel 2019 coronavirus outbreak. *Proceedings of the National Academy of Sciences* **117**, 7504–7509 (2020).

[64] Di Domenico, L., Pullano, G., Pullano, G., Hens, N. & Colizza, V. Expected impact of school closure and telework to mitigate COVID-19 epidemic in france. *EPIcx Lab* **15** (2020).

[65] Herbrich, R., Rastogi, R. & Vollgraf, R. Crisp: A probabilistic model for individual-level COVID-19 infection risk estimation based on contact data (2020). 2006.04942.

[66] Kucharski, A. J. *et al.* Effectiveness of isolation, testing, contact tracing, and physical distancing on reducing transmission of SARS-CoV-2 in different settings: a mathematical modelling study. *The Lancet Infectious Diseases* **20**, 1151–1160 (2020).

[67] Aleta, A. *et al.* Modelling the impact of testing, contact tracing and household quarantine on second waves of COVID-19. *Nature Human Behaviour* **4**, 964–971 (2020).

[68] Barbosa, H. *et al.* Human mobility: Models and applications. *Physics Reports* **734**, 1–74 (2018).

[69] Duque, D. *et al.* Timing social distancing to avert unmanageable COVID-19 hospital surges. *Proceedings of the National Academy of Sciences* **117**, 19873–19878 (2020).

[70] Block, P. *et al.* Social network-based distancing strategies to flatten the COVID-19 curve in a post-lockdown world. *Nature Human Behaviour* **4**, 588–596 (2020).

[71] Simini, F., González, M. C., Maritan, A. & Barabási, A.-L. A universal model for mobility and migration patterns. *Nature* **484**, 96–100 (2012).

[72] Yan, X.-Y., Zhao, C., Fan, Y., Di, Z. & Wang, W.-X. Universal predictability of mobility patterns in cities. *Journal of The Royal Society Interface* **11**, 20140834 (2014).

[73] Jankowiak, M. & Gomez-Rodriguez, M. Uncovering the spatiotemporal patterns of collective social activity. In *Proceedings of the 2017 SIAM International Conference on Data Mining*, 822–830 (SIAM, 2017).

[74] Zarezade, A., Jafarzadeh, S. & Rabiee, H. R. Recurrent spatio-temporal modeling of check-ins in location-based social networks. *Plos one* **13**, e0197683 (2018).

[75] Zhou, K., Zha, H. & Song, L. Learning triggering kernels for multi-dimensional hawkes processes. In *International Conference on Machine Learning*, 1301–1309 (PMLR, 2013).

[76] Xu, H., Farajtabar, M. & Zha, H. Learning granger causality for hawkes processes. In *International Conference on Machine Learning*, 1717–1726 (PMLR, 2016).

[77] Upadhyay, U., De, A. & Gomez-Rodriguez, M. Deep reinforcement learning of marked temporal point processes. In *NeurIPS* (2018).

[78] Zuo, S., Jiang, H., Li, Z., Zhao, T. & Zha, H. Transformer hawkes process. In *International Conference on Machine Learning*, 11692–11702 (PMLR, 2020).

[79] Du, N. *et al.* Recurrent marked temporal point processes: Embedding event history to vector. In *Proceedings of the 22nd ACM SIGKDD International Conference on Knowledge Discovery and Data Mining*, 1555–1564 (2016).

[80] Farajtabar, M. *et al.* Coevolve: A joint point process model for information diffusion and network evolution. *The Journal of Machine Learning Research* **18**, 1305–1353 (2017).

[81] Nanni, M. *et al.* Give more data, awareness and control to individual citizens, and they will help COVID-19 containment. *Ethics and Information Technology* 1–6 (2021).

[82] Troncoso, C. *et al.* Decentralized privacy-preserving proximity tracing (2020).

[83] Nishiura, H. *et al.* Estimation of the asymptomatic ratio of novel coronavirus infections (COVID-19). *International journal of infectious diseases* **94**, 154 (2020).

[84] Lavezzo, E. *et al.* Suppression of a SARS-CoV-2 outbreak in the italian municipality of Vo'. *Nature* **584**, 425–429 (2020).

[85] Tindale, L. *et al.* Transmission interval estimates suggest pre-symptomatic spread of COVID-19. *MedRxiv* (2020).

[86] World Health Organization. Report of the who-china joint mission on Coronavirus disease 2019 (COVID-19). `https://www.who.int/docs/default-source/coronaviruse/who-china-joint-mission-on-{COVID-19}-final-report.pdf` (2020).

[87] He, X. *et al.* Temporal dynamics in viral shedding and transmissibility of COVID-19. *Nature medicine* **26**, 672–675 (2020).

[88] Woelfel, R. *et al.* Clinical presentation and virological assessment of hospitalized cases of coronavirus disease 2019 in a travel-associated transmission cluster. *MedRxiv* (2020).

[89] Wang, D. *et al.* Clinical characteristics of 138 hospitalized patients with 2019 novel coronavirus–infected pneumonia in wuhan, china. *Jama* **323**, 1061–1069 (2020).

A Household Exposures

If information about households $\mathcal{H}(i)$ that each individual $i \in \mathcal{V}$ belongs to is available, one can account for exposures within households analogously to exposures at sites $\mathcal{S}$ by adding an additional rate $\lambda_{\mathcal{H}(i)}(t)$ to the conditional intensity function $\lambda_i^*(t)$ of the exposure counting process $N_i(t)$:

$$\lambda_{\mathcal{H}(i)}(t) = \xi \sum_{j \in \mathcal{H}(t) \setminus i} \int_{t-\delta}^{t} K_{i,j}^{\mathcal{H}}(\tau)\, \gamma e^{-\gamma(t-\tau)} d\tau \tag{9}$$

where

$$K_{i,j}^{\mathcal{H}}(\tau) = \Big(I_j^s(\tau) + I_j^p(\tau) + \mu I^a(\tau) \Big) \prod_{k \in \mathcal{S}} (1 - P_{i,k}(\tau))(1 - P_{j,k}(\tau)) \tag{10}$$

where $\xi \geq 0$ is the base transmission rate within households. This intensity function models our assumption that individuals within a household are in contact as long as they are not visiting any site.

Exposure events caused by $\lambda_{\mathcal{H}(i)}(t)$ can be sampled analogously to the principles for sampling exposure times introduced in Section 3.1. Their superposition with exposures at sites is handled by the priority queue.

B Empirical Probability of Exposure

The exposure risk of others caused by an infectious individual can be computed under our model and empirically approximated using location or contact data, *e.g.*, from (manual) contact tracing. Specifically, the probability of exposure $\hat{p}_{j \leftarrow i}(t_0, t_f)$ during a time window $[t_0, t_f]$ associated with i in the process $N_j(t)$ is given by:

$$\hat{p}_{j \leftarrow i}(t_0, t_f) = 1 - \exp\left(-K_{i,j}^{\text{risk}}(t_0, t_f) \right) \tag{11}$$

with

$$K_{i,j}^{\text{risk}}(t_0, t_f) = \sum_{k \in \mathcal{S}} \beta_k \int_{t_0}^{t_f} P_{j,k}(t') \int_{t'-\delta}^{t'} P_{i,k}(\tau) \gamma e^{-\gamma(t'-\tau)} d\tau dt' \tag{12}$$

and follows from the survival probability in a temporal point process [21].

C State variable initialization

During the parameter estimation period, it is necessary to specify initial epidemiological conditions $\mathbb{S}(0)$ that are consistent with the COVID-19 case data used in the objective. To this end, we set the number of initially symptomatic individuals $I_{\text{init}}^s = \sum_{i \in \mathcal{V}} I^s(0)$ equal to the real observed COVID-19 cases in a region at the start date, or scaled proportionally to the population size in an administrative region, and set all to be positively tested. Based on the above, we seed $I_{\text{init}}^a = \alpha_a / (1 - \alpha_a) I_{\text{init}}^s$ individuals to be initially asymptomatic to obtain a proportion of recently estimated $\alpha_a = 0.4$ asymptomatic seeds [24, 83, 84]. Assuming that infectious individuals have exposed R_0 others on average, we seed $E_{\text{init}} = R_0 (I_{\text{init}}^a + I_{\text{init}}^s)$ initially exposed individuals, using recent estimates of the basic reproduction number of approximately $R_0 \approx 2.0$ [24, 85, 86]. In any simulation done for parameter estimation, $E_i(0), I_i^a(0), I_i^s(0)$ are seeded uniformly at random following the above heuristic counts. Neither asymptomatic nor symptomatic seeds cause further exposures, and for simplicity no other states are initially seeded.

Table 2: Epidemiological model parameters in units of days. Hospitalization and fatality rates α_h and α_b mentioned in the main text are estimated from COVID-19 case data in the region and is age-dependent. Log-normal parameters denote the underlying normal mean and standard deviation.

Counting process	Starts when	$\log\mathcal{N}$ parameters	Source
$M_i(t)$	$dE_i(t) = 1$	$(0.9470, 0.6669)^\dagger$	[26]
$R_i^s(t), R_i^a(t)$	$dI_i^s(t) = 1$	$(2.6365, 0.0713)^\ddagger$	[86–88]
$W_i(t)$	$dI_i^p(t) = 1$	$(0.7463, 0.4161)^\ddagger$	[87]
$Y_i(t)$	$dI_i^s(t) = 1$	$(1.9358, 0.1421)^\ddagger$	[89]
$Z_i(t)$	$dI_i^s(t) = 1$	$(2.5620, 0.0768)^\ddagger$	[27]

	Value	Description	Source
μ	0.55	relative asymptomatic transmission rate	[23]
γ	$6.3013\,h^{-1}$	decay of infectiousness at sites§	[25]
δ	$0.3654\,h$	non-contact contamination window¶	[25]
α_a	0.4	proportion of asymptom. individuals	[24, 83, 84]

† Incubation period from [26], corrected by pre-symptomatic infectiousness [87].
‡ Approximate log-normal parameters constructed because COVID-19 literature results only reported using mean or median time estimates.
§ Assumes that transmission decays with a half-life 10 times shorter than estimated for aerosols under laboratory conditions.
¶ For computational purposes, set from γ by the time when rate of transmission drops below 10% after leaving a site.

Table 3: Assumed mean number of visits per week per site type by individuals of different age groups for our event-based gravity mobility model [22]. See Section 4.1.

Age group	Education	Social	Transport.	Work	Groceries
0-4	5	1	-	-	-
5-14	5	2	3	-	-
15-34	2	2	3	3	1
35-59	-	2	1	5	1
60-79	-	3	2	-	1
80+	-	2	1	-	1

Table 4: Summary and estimated parameters for towns and regions studied in Germany and Switzerland. Recall that β denotes the individual transmission rate at public sites and ξ in households estimated as described in Sections 3.2 and 4.1.

Region	Country	$\lvert\mathcal{V}\rvert$	$\lvert\mathcal{S}\rvert$	Estimation period†	Lockdown	β	ξ
Bern	CH	133,790	2,174	03/06 - 05/10	03/16	0.0337	0.0038
Tübingen	GER	90,539	1,446	03/12 - 05/03	03/23	0.0402	0.0664
Canton Jura	CH	73,416	729	03/09 - 05/10	03/16	0.0131	0.0080
Rheingau-Taunus-Kreis	GER	187,163	2,352	03/10 - 05/03	03/23	0.0010	0.0500
Kaiserslautern	GER	104,044	1,525	03/15 - 05/03	03/23	0.0279	0.0061

† Chosen such that a given region had approximately five to ten confirmed COVID-19 cases, allowing for non-degenerate and comparable initial conditions. Dates are in 2020.

D Estimation Results for Additional Regional Models

Figure 6 summarizes the parameter estimation results for four additional regions in Germany and Switzerland: the cities of Tübingen and Kaiserslautern as well as the Canton of Jura and the district Rheingau-Taunus. As for the model of Bern, the estimation procedure was executed as described in Section 4.1. Table 2 lists the estimated optimal parameters as well as additional details about each regional model.

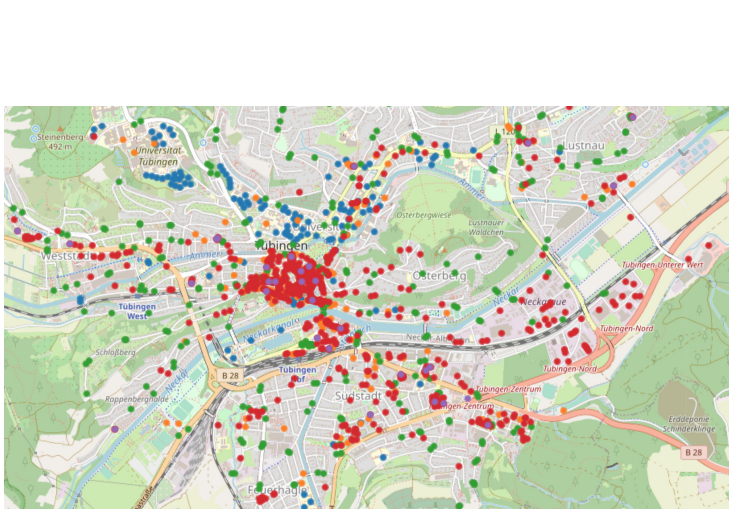

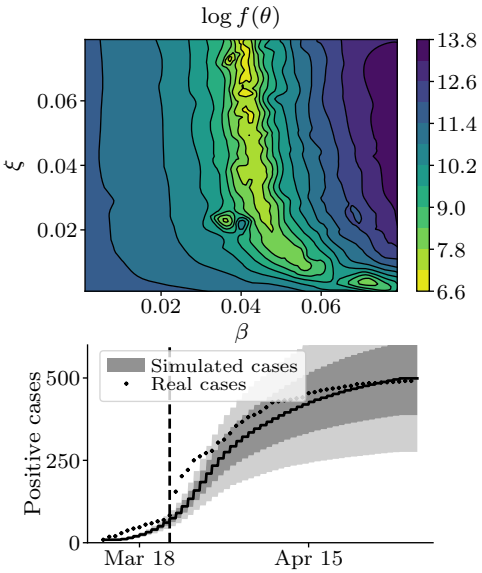

(a) Tübingen, Germany

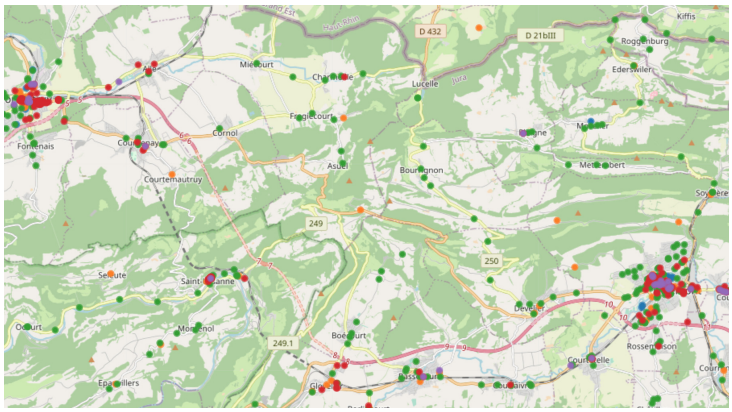

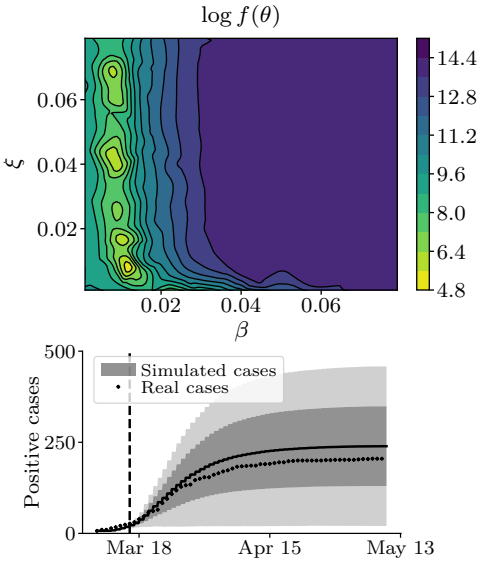

(b) Canton Jura, Switzerland

Figure 6: **Transmission parameter estimation for additional regional models in Germany and Switzerland.** In each panel, the left plot shows the sites of the mobility model with colors used as in Figure 1. The right plots show the contour plot of the log objective in (8) as a function of the transmission rates β and ξ as well as the predicted and real cumulative cases under the estimated parameters, analogous to Figure 2.

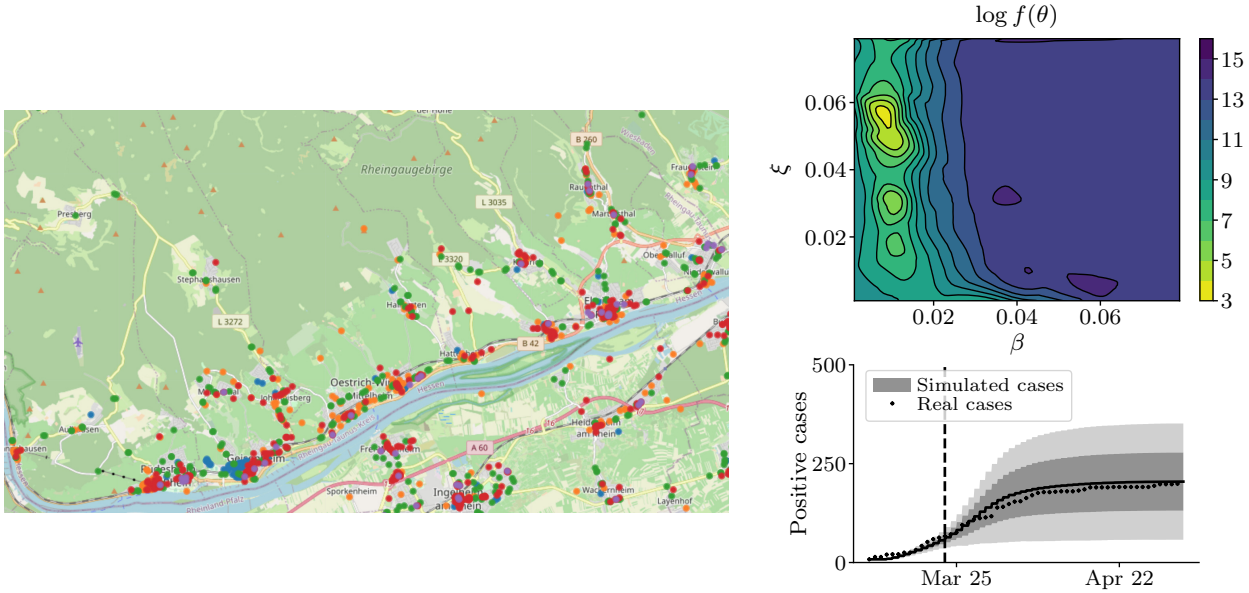

(c) Rheingau-Taunus-Kreis, Germany

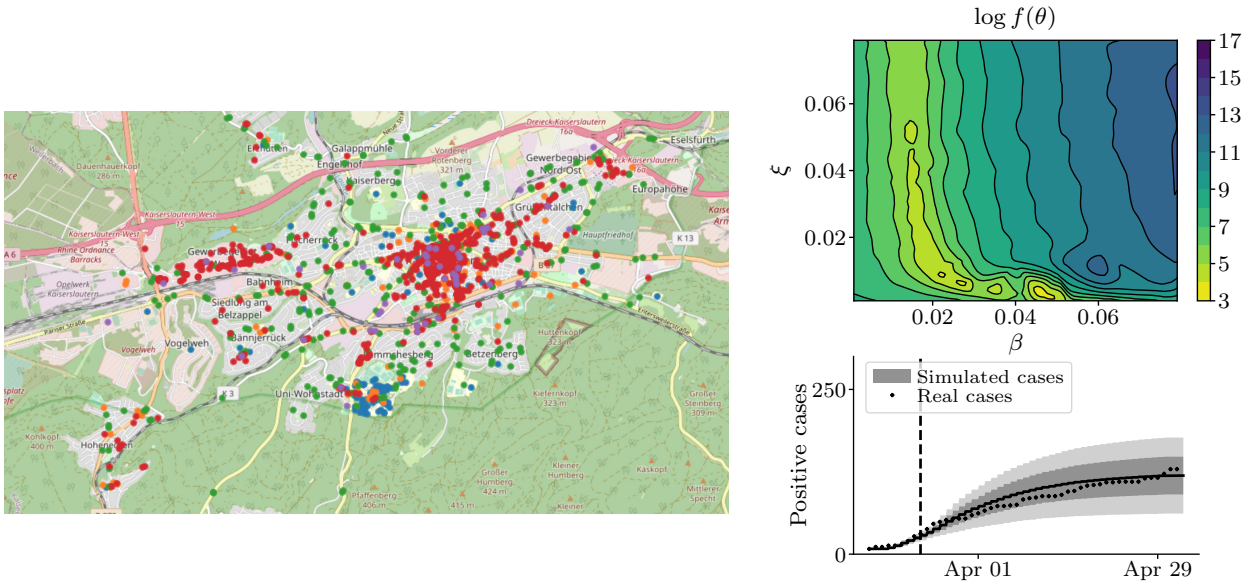

(d) Kaiserslautern, Germany

Figure 6: Continued

E Sampling Algorithms

Algorithm 2 Sampling algorithm for model simulation[5]

Input: Initial state variables at $t = 0$, location traces $P_{i,k}(t)$, parameters γ, δ, α_a, α_b, α_h, μ and β_k, rates $\lambda\_(t)$

$t_{\text{now}} \leftarrow 0$, $S_i \leftarrow 1$, $Q \leftarrow$ priority queue processing in temporal order of events
for all $i \in \mathcal{V}$ s.t. $S_i = 0$ **do**
    Push initial state transition $(0, \_, i, \varnothing, \varnothing)$ to Q (see below)
while Q not empty **do** ▷ Priority queue Q contains $(\text{time}, \text{transition}, i, \text{infector}, \text{site})$ events
    $(t_{\text{now}}, e, i, j, k) \leftarrow$ pop earliest from Q
    if e **is** dE **and** $R_j(t_{\text{now}}) = 0$ **and** $D_j(t_{\text{now}}) = 0$ **and** $S_i = 1$ **then**
        if Interventions$(i, j, k, t_{\text{now}})$ **then** ▷ Reject event and re-sample arrival time of event?
            Call Algorithm 3 with $(P, j, i, t_{\text{now}}, r = 1 - (1 - \mu)I_j^a(t_{\text{now}}))$
        else ▷ Person i exposed by infector j
            $E_i \leftarrow 1$, $S_i \leftarrow 0$, $\Delta_M \sim \text{Expo}(\lambda_M(t_{\text{now}}))$, $u \sim \text{Unif}(0, 1)$
            if $u \leq \alpha_a$ **then**
                Push $(t_{\text{now}} + \Delta_M, dI^a, i, \varnothing)$ event to Q
            else
                Push $(t_{\text{now}} + \Delta_M, dI^p, i, \varnothing)$ event to Q
    else if e **is** dI^p **then** ▷ Person i pre-symptomatic
        $I_i^p \leftarrow 1$, $E_i \leftarrow 0$, $\Delta_Z \sim \text{Expo}(\lambda_W(t_{\text{now}}))$
        Push $(t_{\text{now}} + \Delta_W, dI^s, i, \varnothing)$ event to Q
        for u such that $S_u = 1$ **do**
            Call Algorithm 3 with arguments $(P, i, u, t_{\text{now}}, r = 1)$
    else if e **is** dI^s **then** ▷ Person i symptomatic
        $I_i^s \leftarrow 1$, $I_i^p \leftarrow 0$, $u, v \sim \text{Unif}(0, 1)$
        if $u \leq \alpha_h$ **then**
            $\Delta_Y \sim \text{Expo}(\lambda_Y(t_{\text{now}}))$, Push $(t_{\text{now}} + \Delta_Y, dH, i, \varnothing)$ to Q
        if $v \leq \alpha_b$ **then**
            $\Delta_Z \sim \text{Expo}(\lambda_Z(t_{\text{now}}))$, Push $(t_{\text{now}} + \Delta_Z, dD, i, \varnothing)$ to Q
        else
            $\Delta_R \sim \text{Expo}(\lambda_{R^s}(t_{\text{now}}))$, Push $(t_{\text{now}} + \Delta_R, dR, i, \varnothing)$ to Q
    else if e **is** dI^a **then** ▷ Person i asymptomatic
        $I_i^a \leftarrow 1$, $E_i \leftarrow 0$, $\Delta_R \sim \text{Expo}(\lambda_{R^a}(t_{\text{now}}))$
        Push $(t_{\text{now}} + \Delta_R, dR, i, \varnothing)$ event to Q
        for u such that $S_u = 1$ **do**
            Call Algorithm 3 with arguments $(P, i, u, t_{\text{now}}, r = \mu)$
    else if e **is** dH **then** ▷ Person i hospitalized
        $H_i \leftarrow 1$
    else if e **is** dR **then** ▷ Person i resistant
        $R_i \leftarrow 1$, $I_i^a \leftarrow 0$, $I_i^s \leftarrow 0$, $H_i \leftarrow 0$
    else if e **is** dD **then** ▷ Person i died
        $D_i \leftarrow 1$, $I_i^s \leftarrow 0$, $H_i \leftarrow 0$

[5] For simplicity, we omit details about the procedure Interventions(i, j, k, t), which applies thinning as explained in Section 3.1 due to interventional measures. Details can be found in our publicly available implementation [20].

Algorithm 3 Pushes the next event of individual i exposing individual j in time window $[t, t_{\max}]$ by considering only the contribution $\lambda^*_{i\to j}(t)$ in (6) as described in Section 3.1.

Input: P, i, j, t, r

procedure InContact(u, v, τ)
  return True **if** $\exists k \in \mathcal{S}$ s.t. $P_{u,k}(\tau) = 1$ and $\exists \tau' \in [\tau - \delta, \tau]$ s.t. $P_{v,k}(\tau') = 1$
  else return False
procedure ContactSite(u, v, τ)
  return k **if** $\exists k \in \mathcal{S}$ s.t. $P_{u,k}(\tau) = 1$ and $\exists \tau' \in [\tau - \delta, \tau]$ s.t. $P_{v,k}(\tau') = 1$
  else return $\varnothing$
procedure NextContact(u, v, τ)
  return $\min_{\tau' > \tau} \tau'$ s.t. InContact(u, v, τ')
procedure WillBeInContact(u, v, τ)
  return True **if** $\exists \tau' \in [\tau, t_{\max}]$ s.t. InContact(u, v, τ')]
  else return False
$\tau \leftarrow t$
while WillBeInContact(j, i, τ) **do** ▷ Thinning loop
  $b \leftarrow$ InContact(j, i, τ)
  if not b **then**
    $\tau \leftarrow$ NextContact(j, i, τ)
  $\Delta_{E_j} \sim \text{Expo}\left(\max_k\{\beta_k\}\, r \int_{\tau-\delta}^{\tau} \gamma e^{-\gamma(\tau - v)} dv\right)$
  $\tau \leftarrow \tau + \Delta_{E_j}$
  if InContact(j, i, τ) **then**
    $k \leftarrow$ ContactSite(j, i, τ)
    $p \leftarrow \left(\beta_k \int_{\tau-\delta}^{\tau} \gamma e^{-\gamma(\tau - v)} P_{i,k}(v) dv\right)$
      $/ \left(\max_k\{\beta_k\} \int_{\tau-\delta}^{\tau} \gamma e^{-\gamma(\tau - v)} dv\right)$
    $u \sim \text{Unif}(0, 1)$
    if $u \le p$ **then** ▷ Accept/reject sampled event time
      Push (τ, dE, j, i, k) event to Q
      break